Annual report on research activities 2011

Keio university
Faculty of Science and Tehcnology

Tanabe Photonic Structure Group

A picture of goup members
taken on May 2011

Contents

Foreword

I am much obligated to everyone who is supporting our new group, “Tanabe Photonic Structure Group,” in the department of Electronics and Electrical Engineering, Faculty of Science and Engineering, in Keio University, Japan.

We started our research activities in year 2011 after four Bachelor students are assigned to our group. From a research aspect, we are trying to explore innovative photonic devices that enable to save the power required for signal processing by using the nature of light. On the other hand, as a faculty staff of an educational institution, I am responsible to train young students and researchers to allow them to become an active part in the research and industrial world. Although research and educational activities work closely together, I would like to focus on the research activities in this report.

This year, I enjoyed my research activities with four students. They all showed great capability and worked very hard to start the research *from-scratch*. One constructed a small clean-room (Class 1000), other built a measurement setup, and set up numerical simulation environments. The details can be found in our homepage. In this report, I would like to focus on some of the research topics.

Although it is not long since our group has started, I am appreciating and glad if you find some interest in our research activities.

July, 2012.

Takasumi Tanabe, Associate Professor,
Department of Electronics and Electrical Engineering,
Keio University

Lab Members (Name and their position after graduation)

Assistant Professor

Takasumi Tanabe

Bachelor students: (The class of 2011)

Yohei Ogawa	Continue his education in the Graduate School in Keio University
Takumi Kato	Continue his education in the Graduate School in Keio University
Hiroshi Kudo	Continue his education in the Graduate School in Keio University
Wataru Yoshiki	Continue his education in the Graduate School in Keio University

Research activities

Rigorous analysis of Kerr bistable memory in silica toroid microcavity

Wataru Yoshiki (B4)

We model nonlinear behavior in a silica toroidal microcavity using coupled mode theory and the finite element method and obtain Kerr bistability that does not suffer from the thermo-optic effect by optimizing the fiber-cavity coupling. Our memory might be used for quantum signal processing because we employ both ultra-high *Q* cavity and the Kerr effect.

Key words: Toroid cavity; Optical memory; Kerr effect; Optical bistability; Coupled mode theory;

1. Introduction

Recently, the technologies for manufacturing optical cavities have been developing. As a result, the quality factors of cavities have increased and the fabrication of ultra-high *Q* cavities has become easier. Formerly, it needed very high power to achieve optical bistability. But now, optical bistability can be achieved at relatively low power in ultra-high *Q* cavities.

Some optical memories that employ optical bistability in the cavity have already been reported [1,2]. However, most of these memories are based on the thermo-optic (TO) effect or carrier-plasma effect, and a memory based on the optical Kerr effect has yet to be achieved.

The Kerr effect can modulate the refractive index in a cavity without the absorption of light, so it is more effective than other effects such as the TO effect or carrier-plasma effect. On the other hand, it is known that the Kerr effect is very difficult to use because the refractive index change that it induces is very small. To employ the Kerr effect we have to choose materials that suppress the TO effect and the carrier-plasma effect. These materials should have a large bandgap and a small absorption coefficient and one such material is silica.

This paper proposes the use of a silica toroid microcavity which consists of silica and silicon, and describes a numerical analysis that confirms that a Kerr bistable memory is feasible in a silica toroid cavity. The analysis utilizes coupled mode theory (CMT) and the finite element method (FEM).

2. Numerical modeling

First, we describe our master equation based on the coupled mode theory in a whispering gallery mode (WGM) cavity to obtain the linear and nonlinear transmittance. The structure is shown in Fig. 1(a). Because a two-port system (a side coupled cavity with one waveguide) makes bistable operation difficult to observe, we focus on a side-coupled four-port system throughout this paper. It consists of a toroid (ring) cavity and two waveguides for input and output light. By using CMT [3] and a slow varying envelope (SVE) approximation, we obtain the master equation of the memory, which can express the time change of the envelope of the cavity mode $A(t)$, as follows,

$$\frac{\mathrm{d}A(t)}{\mathrm{d}t} = \left[j\frac{2\pi c}{n_0+\Delta n}\left(\frac{1}{\lambda_0+\delta\lambda}-\frac{1}{\lambda}\right) - \frac{1}{2\tau_{\mathrm{tot}}}\right]A(t) + \sqrt{\frac{1}{\tau_{\mathrm{coup1}}}}e^{j\theta}S_{\mathrm{in}}(t), \tag{1}$$

where $S_{\mathrm{in}}(t)$, λ, λ_0, $\delta\lambda(t)$ c n_o and $\Delta n(t)$ are the envelope of the waveguide mode in the lower waveguide (shown in Fig. 1(a)), the input wavelength, the resonant wavelength of the cavity, the resonant wavelength shift caused by the refractive index change (described later), the velocity of light, the refractive index of silica and the refractive index change in the cavity caused by nonlinear effects, respectively. θ is the relative phase between the cavity mode and the waveguide mode in the lower waveguide and is expressed as,

$$\theta = 4\pi^2\big(n_0+\Delta n(t)\big)(R+r)\left(\frac{1}{\lambda_0+\delta\lambda}-\frac{1}{\lambda}\right) \tag{2}$$

Where *R* and *r* are the major and minor radii of the toroid cavity shown in Fig. 1(b), respectively. τ_{tot} is the total photon lifetime of the cavity and is defined as,

$$\frac{1}{\tau_{\mathrm{tot}}} = \frac{1}{\tau_{\mathrm{abs}}} + \frac{1}{\tau_{\mathrm{loss}}} + \frac{1}{\tau_{\mathrm{coup1}}} + \frac{1}{\tau_{\mathrm{coup2}}} \tag{3}$$

Where τ_{abs}, τ_{loss}, τ_{coup1} and τ_{coup2} are photon lifetimes that correspond to the loss related to the absorption, the loss unrelated to the absorption, and the coupling between the cavity and the lower and upper waveguides, respectively. By using Eqs. (1-3), the output mode from the lower and upper waveguides $S_{\mathrm{out1}}(\mathrm{t})$ and $S_{\mathrm{out2}}(\mathrm{t})$ can be expressed, as follows,

$$S_{\mathrm{out1}}(t) = e^{-j\beta d}\left[S_{\mathrm{in}}(t) - \sqrt{\frac{1}{\tau_{\mathrm{coup1}}}}e^{-j\theta}A(t)\right], \tag{4a}$$

$$S_{\mathrm{out2}}(t) = e^{-j\beta d}\sqrt{\frac{1}{\tau_{\mathrm{coup2}}}}e^{-j\theta}A(t), \tag{4b}$$

where, β and d are the propagation constant and the length of the waveguides, respectively.

Next, we model the refractive index change caused by nonlinear effects. The carrier-plasma effect is negligible in silica due to its large bandgap, thus, only the modeling of the TO and Kerr effects is necessary. Generally the distribution of the light energy is consistent with the whispering gallery (WG) mode. Therefore, taking the spatial dependency into account, we can calculate the distribution of the refractive index changes caused by the TO $\Delta n_{\mathrm{TO}}(x,y,t)$ and Kerr effects $\Delta n_{\mathrm{Kerr}}(x,y,t)$, as

follows

$$\Delta n_{\mathrm{TO}}(x,y,t) = n_0 C_{\mathrm{TO}}\{T(x,y,t) - 300\}, \qquad (5a)$$

$$\Delta n_{\mathrm{Kerr}}(x,y,t) = \frac{2n_2 c}{n_0} \cdot \frac{U_{\mathrm{p}}(t)}{2\pi R} \tilde{I}(x,y). \qquad (5b)$$

Here $T(x,y,t)$, n_2, $U_{\mathrm{p}}(t) = |A(t)|^2$ and $\tilde{I}(x,y)$ are cross-sectional temperature distribution, the nonlinear refractive index, the light energy stored in the cavity and the normalized cross-sectional intensity distribution obtained by the FEM [4] in advance (shown in Fig.1(b)), respectively. Note that $T(x,y,t)$ can also be calculated by using the FEM (COMSOL Multiphysics). Now, by using Eqs. (1)-(5), we can analyze the nonlinear behavior of this optical memory.

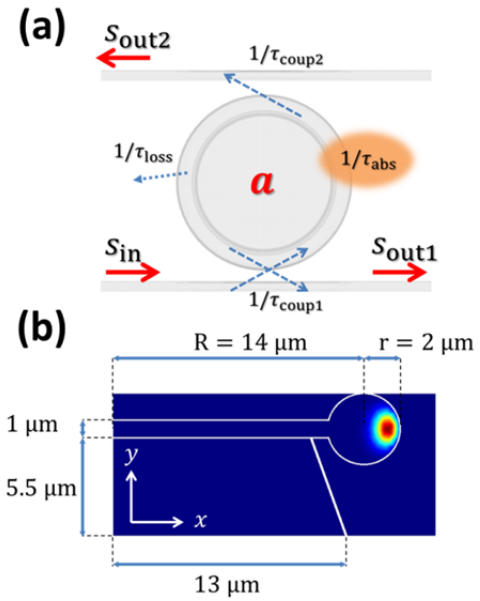

Fig.1: (a) Cavity structure used for numerical analysis. (b) Mode intensity profile of toroid microcavity [4]

3. Determining the photon lifetimes

Here we describe the photon lifetimes that we used in our analysis. The material absorption of silica at telecom wavelengths is usually very small (α = 0.2 dB/km), but, it is known that silica toroid microcavities have much larger absorption due to the water layer and contamination on the surface. And in practice the Q factor is limited by these absorptions. Thus, we decide to consider a realistic case where the experimental Q is limited by the absorption, by setting $\tau_{\mathrm{int}} \approx \tau_{\mathrm{abs}} = 323$ ns (corresponding to $Q_{\mathrm{int}} = 4 \times 10^8$ [5]), where $Q_{\mathrm{int}} = \omega\tau_{\mathrm{int}} = \omega(\tau_{\mathrm{abs}}^{-1} + \tau_{\mathrm{loss}}^{-1})$ is the intrinsic photon lifetime.

In general, as the TO effect is much slower and larger than the Kerr effect, the latter is cancelled out by the former after a certain time. Thus, to use the Kerr effect for the memory, we have to finish the operation before heat has accumulated significantly. The [rising and falling/rise and fall?] time of the energy in the cavity (which is directly related to the operation speed) is determined by τ_{tot}, so, we have to achieve a low τ_{tot} in an ultra-high Q cavity such as a toroid cavity. For this, we decided to control τ_{coup1} and τ_{coup2}. Note that τ_{coup1} is controlled to satisfy $\tau_{\mathrm{coup1}}^{-1} = \tau_{\mathrm{int}}^{-1} + \tau_{\mathrm{coup2}}^{-1}$ and thus achieve critical coupling.

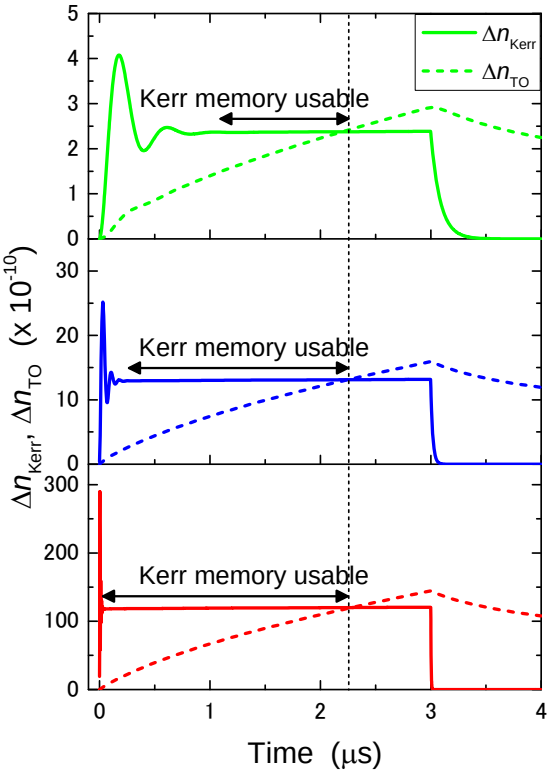

Fig.2: Δn_{Kerr} and Δn_{TO} (broken line) vs. time for different τ_{coup2}. The detuning δ is 27 fm (corresponds to $\sqrt{3}$FWHM).

4. Results and discussions

First, we employ a rectangular pulse to obtain the refractive index change $\Delta n_{\mathrm{TO}}(x,y,t)$ and $\Delta n_{\mathrm{Kerr}}(x,y,t)$. The calculation results are shown in Fig. 2 for three different τ_{coup2} values. The figure shows that $\Delta n_{\mathrm{TO}}(x,y,t)$ is larger than $\Delta n_{\mathrm{Kerr}}(x,y,t)$ in all three cases when t is larger than 2.3 μs. This number gives us the upper limit of the Kerr memory holding time without suffering from the TO effect; namely it is the usable domain for Kerr memory operation, which we call "Kerr usable regime" shown in Fig. 2. Finally, Fig. 2(a) shows that the charging speed of the cavity differs for different τ_{coup2} values. The cavity charging time is much faster for $\tau_{\mathrm{coup2}} = \tau_{\mathrm{int}}/100$, which allows the cavity to reach to a plateau Δn_{Kerr} domain much faster. This enables us to have a longer ``Kerr memory usable'' regime, which allows us to use the cavity for a longer duration as an optical Kerr memory. The figure shows that we can maximize the Kerr dominant "Kerr memory usable" regime by setting τ_{coup2} as small as possible.

Finally, the memory operation for various τ_{coup2} values is shown in Fig. 3. Since the response speed of

$P_{out1} = |S_{out1}|^2$ depends on the total photon lifetime τ_{tot}, we normalized the temporal axis t by τ_{tot}. Figure. 3 shows clearly that the reset pulse does not work when $\tau_{coup2} = \tau_{int}$ and $\tau_{int}/10$, and the memory operation cannot be obtained at this condition. If the system is operating at the Kerr dominant regime, we should be able to reset the state by injecting a negative reset pulse. The required pulse width needed for the reset pulse is $> \tau_{tot}$, since we can discharge the cavity within this time. However, the figure shows that significant heat is accumulating in the system, which makes the system impossible to reset because Δn_{TO} cannot be reset by such a short negative pulse due to its much longer relaxation time.

On the other hand, when $\tau_{coup2} \leq \tau_{int}/100$, we can successfully set and reset the system, and use the device as a Kerr bistable memory. However, the TO effect cannot be eliminated completely even in this case, and thus a holding time exists. It automatically switches P_{out1} from ON to OFF due to the thermal accumulation. Figure 3 shows that the memory holding time for a realistic case is about 500 ns.

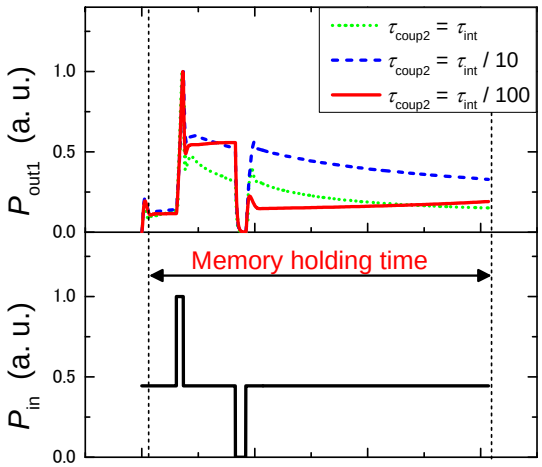

Fig. 3: Optical memory operation, when δ is $\sqrt{3}$FWHM. The input power of the drive light is2 μW, 80 μW and 7.3 mW, when $\tau_{coup2}$is τ_{int}, $\tau_{int}/10$ and $\tau_{int}/100$, respectively. The horizontal axis is normalized with the photon lifetime τ_{tot}.

5. Conclusion

We rigorously modeled the Kerr and TO effects in a silica toroid microcavity by combining CMT and FEM. A clear understanding was gained of the impact on adjusting the coupling, and showed that Kerr optical bistable memory operation is possible by adjusting the coupling between the cavity and the waveguides. The memory holding time is about 500 ns. Although the driving power is 7.3 mW, the energy consumed by the system is extremely low. This is because Kerr nonlinearity does not absorb photons, while other nonlinearities such as carrier or TO effects do. In addition, due to the ultrahigh-Q of the system, the energy loss outside the system is also low. Our Kerr bistable memory in a silica toroidal microcavity has extremely low loss and thus is suitable for such applications as quantum signal processing.

References

[1] T. Tanabe, M. Notomi, S. Mitsugi, A. Shinya, and E. Kuramochi, Appl. Phys. Lett. **87**, 151112 (2005)..

[2] V. Almeida and M. Lipson, Opt. Lett. **29**, 2387–2389 (2004).

[3] C. Manolatou, M. Khan, S. Fan, P. Villeneuve, H. Haus, and J. Joannopoulos, IEEE J. Quantum Electron. **35**, 1322–1331 (1999).

[4] M. Oxborrow, IEEE Trans. Microw. Theory Tech. **55**, 1209–1218 (2007).

[5] T. Kippenberg, S. Spillane, and K. Vahala, Appl. Phys. Lett. **85**, 6113–6115 (2004).

Method of fabricating high transmission optical tapered fiber

Yohei Ogawa (B4)

Optical tapered fiber is an essential tool for measuring the optical characteristics of microcavities. In this paper, we describe the fabrication of the tapered fiber that transmits 70% of the input power and that provides a 20 dB evanescent light. We confirmed the results both theoretically and experimentally.

Keywords : Tapered fiber, Optical waveguide, Evanescent light

1. What is optical tapered fiber?

In recent years, optical microcavities have been intensively researched. The Q factor is often used to show the performance of the microcavity system. When measuring the Q factor we must couple light into a microcavity by evanescent light. An optical tapered fiber is an ideal tool because it can excite evanescent light.

Optical tapered fiber is shown schematically in Fig.1.

We can fabricate tapered fiber by pulling heated single mode fiber (SMF) until its diameter is about 1 μm. Because the fiber diameter is about the same as the optical wavelength 1.55 μm, a large part of the mode leak outside the fiber core and excite evanescent field. We can use this light to excite the whispering gallery mode of microcavities.

In this paper, we first estimated the amount of the leakage of the evanescent light into the air in respect to the fiber diameters. Then I show the fabrication of an ideal tapered fiber.

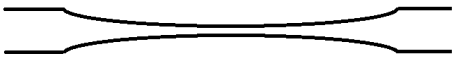

Fig. 1. Schematic illustration of tapered fiber.

2. Estimating taper diameter

To fabricate optical tapered fiber, we need to determine its shape. And we must obtain the diameter of the tapered fiber at a particular point. First, we consider only a small region, which is heated with an LPG flame. When the state k (at time t) changes to $k+1$, at a constant volume, we obtain

$$\pi r_k^2 L = \pi(r_k + \Delta r)(L + \Delta l) \quad (1)$$

where r_k is the fiber radius, L is the length of the region that the flame crosses, and $\Delta r, \Delta l$ is the difference between r and L. Formula (1) is deformed to

$$r_{k+1} = r_k + \Delta r = r_k \sqrt{\frac{L}{L + \Delta l}} \quad (2)$$

If t is not continuous, cylinders will be formed whose radius is r_k and whose length is $\frac{\Delta l}{2}$. This is shown in Fig. 3. Because the pull time t is continuous, the shape of the tapered fiber is as shown in Fig. 1. We used a pulling speed $v = 240$ μm/ s, a heating length $\mathrm{L} = 3$ mm and a step time $\mathrm{t} = 0.1$ s/step. These values lead to $\Delta l = vt = 24$ μm/step. After comparing experimental results, we chose the $L = 3$ mm graph for our method. We estimate the pull time needed to fabricate an arbitrary diameter using this function.

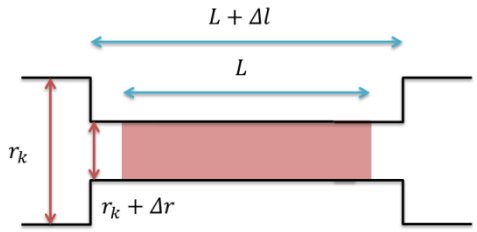

Fig. 2. Heated region of tapered fiber. Radius and length change is described.

Fig. 3. Image of tapered fiber according to eq. (2).

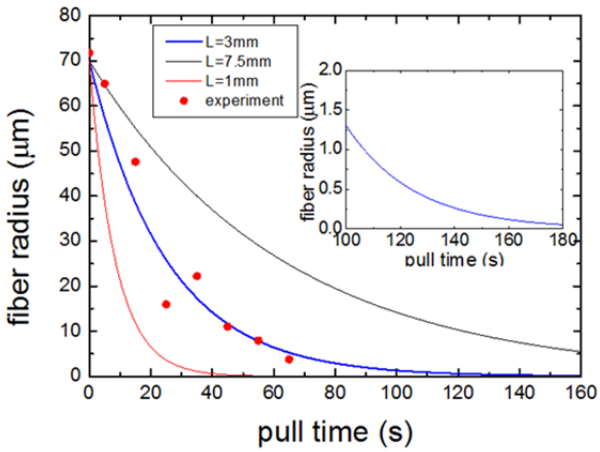

Fig. 4. Minimum radius of optical tapered fiber versus pull time.

Next, we performed a mode propagation simulation with RSoft BeamPROP. The light power near the tapered fiber is shown in Fig. 5. According to Fig. 5, a tapered fiber with $d = 600$ nm can provide a 40% evanescent light from the input light. This is sufficient to introduce light into a microcavity when our target was to fabricate $d = 600$ nm tapered fiber.

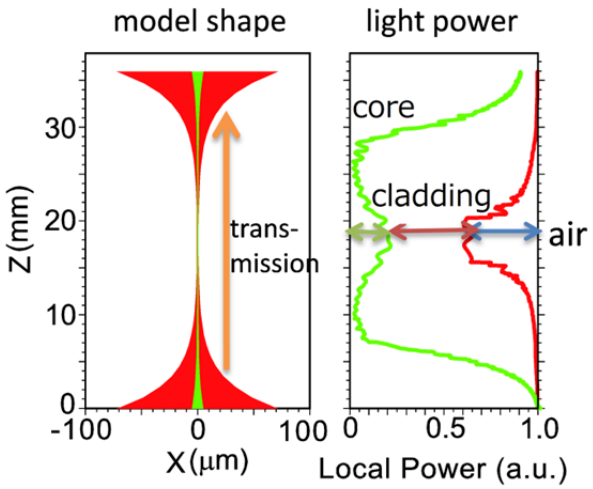

Fig. 5. Left: Simulated tapered fiber shape. Right: Propagated length versus light mode power.

3. Construction of flame temperature

When fabricating optical tapered fiber, the temperature of the flame used in the process is an important factor. The temperature of an LPG flame can be estimated from the LPG and O_2 gas flow rates and from the mixture rate of the two gases. According to previous reports [1,2], the glass processing temperature is 1900 ~ 2100 K. To achieve this flame temperature requires an LPG and O_2 molecular ratio of 2.8:5 [3]. When LPG is burnt at this ratio CO and CO_2 are generated but not soot. In this work, the LPG pressure was 0.0686 MPa and the pressure was 0.1 MPa. These pressures and molecular ratios result in a 7:10 flow ratio. We adopted this ratio for the LPG and O_2 gas.

4. Fabrication optical tapered fiber

The equipment for fabricating optical tapered fiber is shown in Fig. 6. A schematic diagram is shown in Fig. 7. The optical fiber is heated by an LPG burner located in the center and pulled at a constant speed by an automatic sample stage.

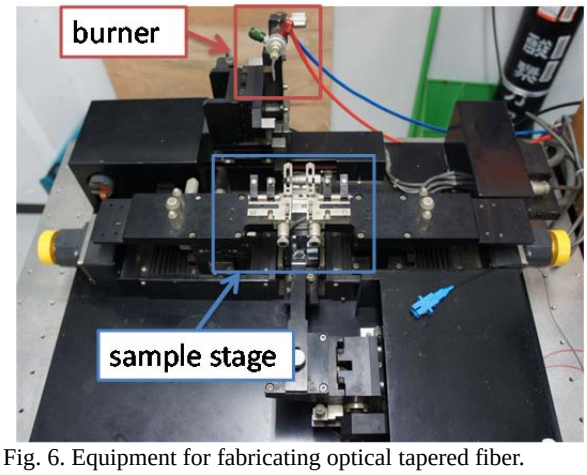

Fig. 6. Equipment for fabricating optical tapered fiber.

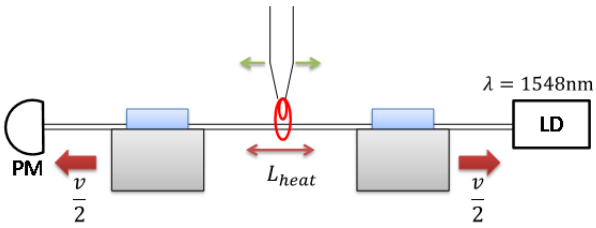

Fig. 7. Making method.

We fabricated the optical tapered fiber while observing the laser transmission. The gas ratio was set as discussed in section 3. The LPG pressure was 0.0686 MPa, the flow rate was $14\ \mathrm{ml/min}$, the O_2 gas pressure was 0.1 MPa, and the flow rate was $20\ \mathrm{ml/min}$. If we want to fabricate $d = 600\ \mathrm{nm}$ tapered fiber, when the pulling speed is set at $v = 240\ \mu\mathrm{m/s}$, the estimated pull time is $t = 150\ \mathrm{s}$ from Fig. 4. With this requirement we observed light transmission $\lambda = 1550\ \mathrm{nm}$ while optical tapered fiber fabrication, described in Fig. 8. It shows that optical tapered fiber can be stably fabricated and the transmission loss is about 2 dB.

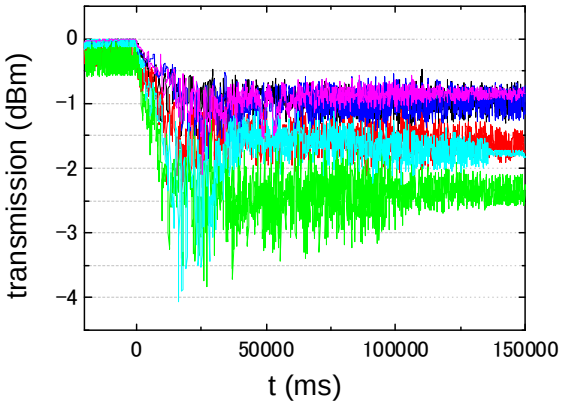

Fig. 8. Transmission power when pulling fiber. Input wavelength is $\lambda = 1550$ nm.

Fig. 9 shows the transmission loss when the optical tapered fiber touches the slide glass. The observed 10 dB loss shows that a lot of light escapes from the tapered fiber.

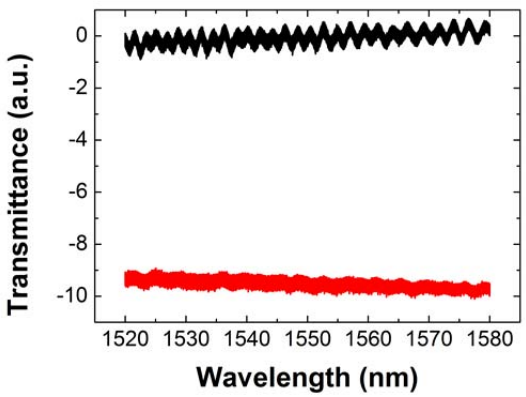

Fig. 9. Spectrum of tapered fiber. Black: Nothing touching tapered fiber. Red: Touching slide glass.

5. Conclusion

In this paper, I showed how to fabricate optical tapered fiber for measuring microcavities and described the optical characteristics of optical fiber.

6. References

[1] S. Sakuka, “Basis and application of the science of glas,” Uchida Rokakuho (1997) (in Japanese)
[2] D. G. Holloway, K. Ooi translated, “Physics of Glass” Kyoritsu Publishing (1977) (in Japanese)
[3] K. Shuzenji, Fukuoka Industrial Technology Center Research Expenses **18**, 25 (2008)

Constructing a laser reflow system and fabricating silica toroid microcavities

Watary Yoshiki (B4) Takumi Kato (B4)

In this work, we constructed a system for performing a laser reflow process, which is an important part of silica toroid microcavity fabricating process. Furthermore, we successfully fabricated a silica toroid microcavity by performing a laser reflow process on a disk structure fabricated in a clean room. As a result, we have been able to use the cavities for various applications.

Key words: Silica toroid microcavity; laser reflow; CO_2 laser.

1. Introduction

Rrecent progress on the technology used to fabricate optical micro cavities has made it easy to fabricate ultra-high *Q* cavities. As the light is strongly confined in such a cavity, an interaction between the light and matter can be easily obtained. As a result, we can use various optical nonlinear effects efficiently within the cavities.

A silica toroid microcavity was proposed by Vahala's group in 2003 [1]. The characteristic of this kind of cavity is an ultra-high *Q* and the highest reported value is 4×10^8 [2]. This is a much higher *Q* than can be obtained with a silicon microring resonator ($Q = 1.43 \times 10^5$) [3] or a photonic crystal ($Q = 1.43 \times 10^5$) [4]. Although silica microsphere cavities have much higher *Q* value of $> 10^9$ [5], a toroid cavity has a superior capacity for integration on a chip because it can be fabricated on a Si chip. So it has been used for many applications related to lasers, sensors and cavity quantum electro dynamics (QED).

In this work, we constructed a system for performing a laser reflow process, which is an important part of the procedure used for fabricating silica toroid microcavities, in order to study the application of the cavity. We successfully achieved the trial fabrication of a silica toroid microcavity, and we are now ready to study its application.

2. Fabricating process of a silica microcavity

This section details a method for fabricating a silica toroid microcavity. First, a silica pad is fabricated on silicon on insulator (SOI) chip by photolithography. Then, Si under the pad is selectively removed by XeF_2 dry etching. After that a silica disk on a silicon pillar is obtained as shown in Fig. 1. Although this disk structure can be used as an optical cavity, laser reflow is performed on the structure to achieve a much higher quality factor. Laser reflow is a process whereby the fringe area of the silica is melted with a CO_2 laser. The silica disk shrinks during this process and a silica toroid microcavity is realized. The entire process is shown in Fig. 1.

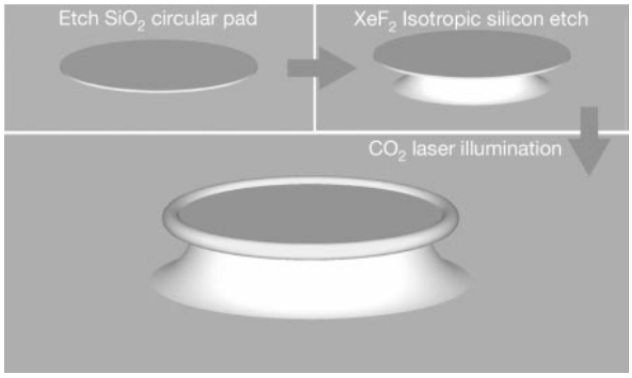

Fig. 1：Flow diagram illustrating the process used to fabricate silica toroid microcavities[1].

The fringe area of the silica disk can be selectively melted because 1) silica has a much larger absorption coefficient than Si in a wavelength of 10.6 μm and 2) Si has a larger thermal conductivity than silica. While the CO_2 laser is focused on the disk structure, a large amount of heat is generated in the silica disk due to its large absorption coefficient. Although the heat generated in the central area of the disk flow through the Si pillar, which has large thermal conductivity, heat generated in the fringe area of the silica disk accumulates because the area is thermally isolated by the surrounding air. Therefore, only the fringe area is heated toward its melting point, and this causes it to shrink.

To feed light into the cavity, a tapered optical fiber is brought near the cavity until it is less than 1 μm from it. Subsequently, the light in the evanescent field is inputted into a torus-shaped part of the cavity and looped circularly within the cavity. This loop is the principle to confine the light in the silica toroid microcavity. Although there is surface roughness on the silicon microring cavity or photonic crystal caused by the etching process, a silica toroid microcavity has a smooth surface because laser reflow is performed after etching and surface tension makes the surface very smooth. So the surface scattering loss decreases greatly and the *Q* of the toroid cavity increases greatly. Therefore, laser reflow is a very important process for obtaining an ultra-high quality factor.

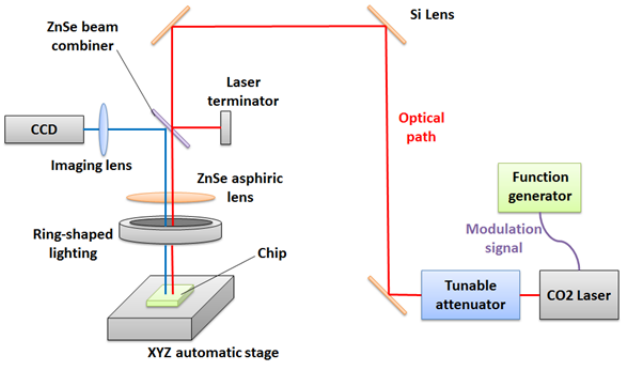

Fig. 2：Experimental set-up for reflow process.

3. Construction of laser reflow system

This section describes the laser reflow system that we constructed. As mentioned in the previous section, we employed a CO_2 laser as a light source. Although the light emitted from CO_2 laser is invisible because of its wavelength of 10.6 μm, a guide laser emitting at a wavelength of 780 nm is attached to coincide with the optical path of the CO_2 laser. Furthermore, the wave shape is modulated to an arbitrary frequency up to 15 kHz by a connected function generator.

The entire optical path within the system is shown in Fig. 2. The beam outputted from the laser is first attenuated down to an appropriate power level through a variable optical attenuator. The beam is then focused on a chip through a ZnSe beam combiner and a ZnSe aspheric lens. As the diameter of the disk structure on the chip is approximately 100 μm, the highly precise alignment of the positions of the disk structure and the laser spot is necessary. Thus, we employed an XYZ automatic stage with a resolution of 100 nm in the xy directions and 10 nm in the z direction.

To confirm that that the laser spot is focused precisely on the disk structure, we constructed the imaging system shown in Fig. 2. In this system, a CCD can capture the reflected light on the chip, so, a clear image can be obtained. Furthermore, as the focal length of the ring-shaped lighting is designed to coincide with that of the ZnSe aspheric lens, the emitted light is efficiently concentrated on the chip. The captured image is shown in Fig. 3(a).

Note that light scattered from a chip is unsafe because of the high power CO_2 laser used for laser reflow. Therefore, we enclosed the stage holding the chip in an aluminum box as shown in Fig. 3(b). In addition to maintain the safety, this box has an additional purpose, which is to increase the air-tightness in the box. It is known that hydroxyls adhere to the surface of the silica toroid microcavity as a result of laser reflow in the air, and so the *Q* of the cavity is decreased [5]. Considering this effect, we plan to conduct the laser reflow in a N_2 atmosphere in the future. This aluminum box is an important step in this respect.

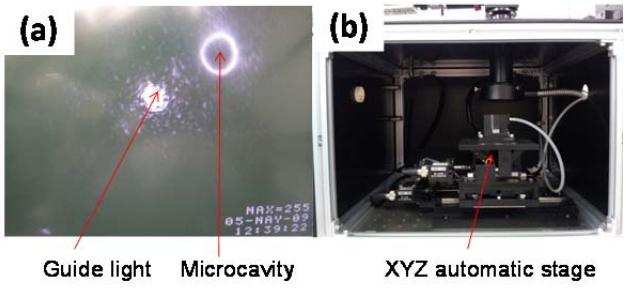

Fig. 3：(a) CCD image. (b) XYZ automatic stage in aluminum box.

4. Fabrication of silica toroid microcavity

This section describes the fabrication of a silica toroid microcavity. Figure 4(a) shows a scanning micro electron microscope (SEM) image of the disk structure prior to laser reflow. This disk structure was made by wet etching for 30s with a mixture ratio of HF : HNO_3 : CH_3COOH = 3 : 5 : 3 and its diameter was 94.8 μm. A SEM image of the structure after the laser reflow is shown in Fig. 4(b). We used an 8 W rectangular laser pulse with a width of 0.75 ms. A comparison of the images obtained before and after laser reflow shows that the fringe area has shrunk and the diameter has decreased from 94.8 to 84.4 μm. From this result, we can conclude that we successfully fabricated a silica toroid cavity with our laser reflow system.

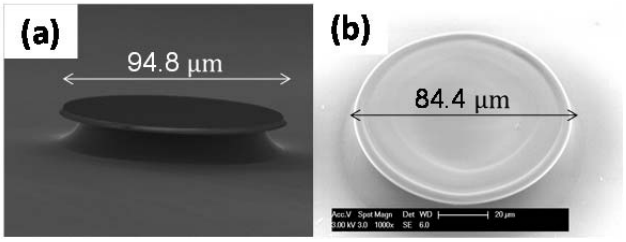

Fig. 4：(a) Disk-shaped structure. (b) Silica toroid microcavity.

In this section, we discuss some of the problems with our laser reflow system. The most significant problem is the distortions of the shape after the laser reflow caused by the invisibility of the CO_2 laser beam spot. We used a guide laser spot to match the spot of the CO2 laser and the disk structure. However, there was a slight disagreement between the optical path of the CO2 laser beam and the guide beam, so a situation where the CO2 laser spot is not perfectly centered on the disk can easily occur. This small error seriously affects the shape after the laser reflow because the disk diameter of approximately 100 μm is very small. As a result, the toroid shape is distorted and this can be the main cause of a decreased *Q* factor. There is an additional problem, namely that hydroxyls and contaminants on the toroid reduce the Q value because we conduct the laser reflow in air. Thus, the measured *Q* of the toroid cavity we fabricated is 3×10^5 and this is a much smaller than the previously reported value [2]. To improve the *Q* factor, next year we will conduct the laser reflow in a N_2 atmosphere.

5. Conclusion

We constructed a system that can perform a laser reflow process for a silica toroid microcavity. Furthermore, we successfully fabricated a silica toroid microcavity by using this system. Next year, we intend to improve the accuracy of the reflow system and study the application of the silica toroid microcavity.

References

[1] D. Armani, T. Kippenberg, S. Spillane and K. Vahala, Nature **421**, 925–928 (2003).
[2] T. Kippenberg, S. Spillane and K. Vahala, Appl. Phys. Lett. **85**, 6113-6115 (2004)
[3] Q. Xu, P. Dong, and M. Lipson, Nat. Phys. **3**, 406–410 (2007)
[4] T. Tanabe, M. Notomi, E. Kuramochi, A. Shinya, and H. Taniyama, Nat. Photonics **1**, 49–52 (2007).
[5] M. Gorodetsky, A. Savchenkov, V. Ilchenko and H. Kimble, Opt. Lett. **21**, 453-455 (1996)

Fabrication and analysis of polygonal silica toroid microcavity

Takumi Kato(B4)　Wataru Yoshiki(B4)

We fabricated polygonal silica toroidal microcavities, which are different from conventional circular cavities. The polygonal cavities were fabricated using a combination of isotropic etching, anisotropic etching and laser reflow. We also simulated these polygonal structures using the two-dimensional finite-difference time domain method.

Key word: Optical microcavity, Semiconductor process, Laser reflow, Polygonal structure, 2D-FDTD

1. Introduction

A silica toroidal microcavity has an ultra-high quality factor (Q) and a small mode volume (V). High-Q microcavities are being studied for use in applications such as biomolecule sensing [1], optical frequency comb generation [2] and optical bistability memory [3]. These applications are still in the research stage because it is hard to couple light between a microcavity and a waveguide. We must use a tapered fiber as a waveguide to couple light to a microcavity because a silica toroidal cavity is a whispering gallery mode (WGM) cavity, which confines light using total internal reflection (TIR), and so we must use an evanescent wave to excite these modes. The use of a tapered fiber needs sensitive control to achieve critical coupling between the cavity and the fiber. The purpose of this research is to solve this coupling problem.

Coupling problems often occur in the microcavity field. One example solution involves a silicon microring [4]. The authors of Ref. 4 fabricated a racetrack shaped silicon microring and increased the coupling length to stabilize the coupling effect. We applied this concept to a silica toroid microcavity and tried to fabricate a polygonal shaped cavity to realize practical use.

2. Silica toroid microcavity fabrication process

2.1 Theory

In 2003, a Caltech team proposed a silica toroid microcavity [5]. There are four main processes (Fig. 1).

1. Grow a thermal dioxide layer on a silicon wafer.
2. Transfer a pattern to a silicon dioxide layer using photolithography.
3. Make a silica disk structure using XeF_2 dry etching, which is the sacrificial etching of silicon.
4. A CO_2 laser melts the silica disk and the edge of the silica disk solidifies.

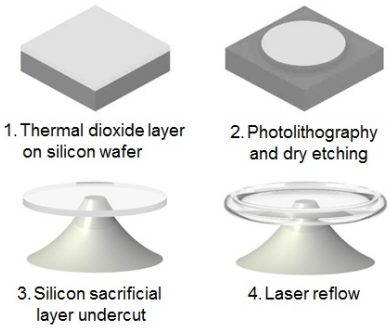

Fig. 1: Silica toroidal microcavity fabrication process.

Here, it is important that the silica toroidal structure depends on the silicon post structure because the silicon post works as heatsink. So, the silicon post pattern may transfer the heat profile to the silica disk. We focused on this relation between the heat profile and the silicon post shape, and set a target to allow control of the structure of the silica toroid microcavity by changing the silicon post shape.

2.2 Experiment

The shape of the silicon post depends on the sacrificial etching. XeF_2 gas commonly is used for this process. XeF_2 is known to be an isotropic etchant for silicon, so we can make a circular silicon post when we use XeF_2 gas.

In our work, we proposed using wet etching (HNA or KOH) to replace XeF_2 gas dry etching.

(1) XeF_2 gas dry etching

XeF_2 gas is commonly used in the sacrificial etching process when fabricating a silica toroid microcavity. Figure 2 shows the silica microdisk after XeF_2 etching.

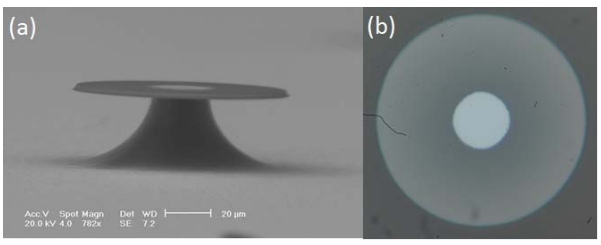

Fig. 2: XeF_2 gas dry etching. (a) SEM image. (b) optical microscope image of a disk cavity with a circular silicon post, fabricated using XeF_2 isotropic etching.

(2) HNA wet etching

We used an HNA mixture (Hydrofluoric (HF), nitric (HNO_3), acetic (CH_3COOH) acids) to make the silica toroid. HNA is known to be an isotropic etchant; however, it has not been used to fabricate a silica toroid. The HNA

mixture is cheaper than XeF_2 gas and the experimental setup is also simpler. So, if we can use this mixture for the fabrication process, the fabrication cost will be very reasonable.
The chemical formula of this reaction is as follows.

$$Si + 2HNO_3 \rightarrow SiO_2 + 2HNO_2 \quad (1)$$

$$SiO_2 + 6HF \rightarrow H_2SiF_6 + 2H_2O \quad (2)$$

This reaction has two processes. The first is the oxidation reaction for silicon. The second is the melting reaction induced by hydrofluoric acid. To make a silica toroid, we need a silica disk after sacrificial etching. However, the second process melts silica. So, we focused on the quality of the thermal oxide film and researched the etching rate of silicon and thermal oxide film. We selected a proper ratio for the mixture ($HF:HNO_3:CH_3COOH$=3:5:3). Experimental etching rate results are shown in Fig. 3.

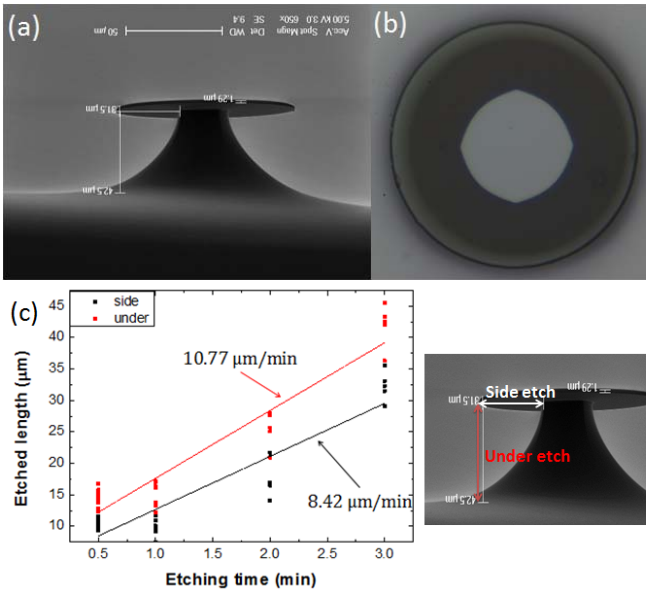

Fig. 3: HNA wet etching: HF (49%) : HNO_3 (70%) : CH_3COOH (99%) = 3:5:3. (a) SEM image (etching time 3 min.). (b) Optical microscope image of a disk cavity with a circular silicon post, fabricated using HNA isotropic etching (etching time 3 min.). (c) Experimental results of HNA (3:5:3) etching.

(3) KOH wet etching

Potassium hydroxide (KOH) is used for the anisotropic etching of the crystalline structure of silicon. There are certain etchants that are used for the anisotropic etching of silicon. For example, tetramethylammonium hydroxide (TMAH), and ethylene diamine and pyrocatechol (EDP).
In this work, we chose KOH and we show our experimental results in Fig. 4.

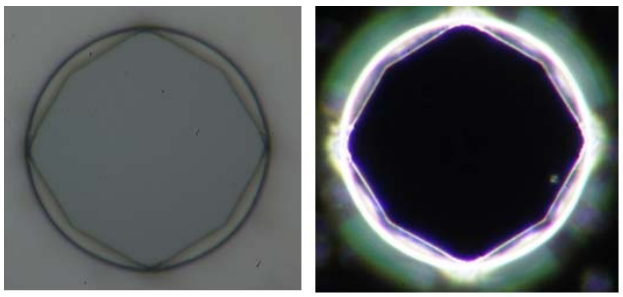

Fig. 4: KOH wet etching. Optical microscope image of a disk cavity with a polygonal silicon post, fabricated using KOH anisotropic etching (4 hour 30 min.).

2.3 Fabricating silica toroid with polygonal structure

From the experimental results in section 2.2, we thought it possible to fabricate a silica toroid with a polygonal structure. We can obtain an octagonal silicon post by using KOH wet etching, however the horizontal etch rate is very slow. So, we cannot make a silica toroid because we need the floating edge of a silica disk when we employ CO_2 laser reflow.

Here, we propose a combination of isotropic and anisotropic etching to realize an octagonal silicon post and a floating silica disk. Figure 5 shows our experimental results.

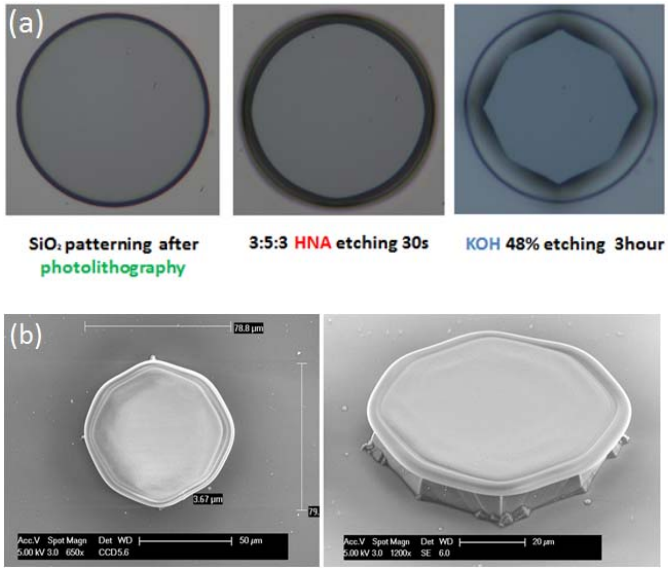

Fig. 5: Fabrication of a polygonal silica toroidal microcavity. (a) Optical microscope image of an octagonal silicon post fabrication. (b) SEM image of a fabricated octagonal toroidal cavity after the laser reflow. The toroid diameter is about 80 μm. A 12-W CO_2 laser is irradiated for 1.5 ms. The focus lens has a focal length of 38.1 mm.

In this work, we successfully fabricated an octagonal silica toroid microcavity. We believe a hexagonal shape or square shape can be fabricated by using anisotropic etchants and a mask pattern for photolithography.

3. Analysis of polygonal silica toroid microcavity

Some research has been reported on polygonal microcavities including silicon microdisks [6, 7]. However, these studies cannot be applied to silica toroids because of the different way of confining light. So, we

analyzed the performance of a polygonal silica toroid by using a two-dimensional – finite difference time domain method (2D-FDTD). We simulated octagonal and circular shapes.

3.1 Non-coupled case

First, we simulated the resonance modes of a microcavity without a coupled fiber. The results are shown in Fig. 6. The circular pattern is a common shape and this resonance mode is WGM. WGM provides strong light confinement. The calculated quality factor was $Q > 10^7$ from this result (a). The resonance mode of the octagonal pattern is a WGM-like mode. Here the calculated quality factor was $Q = 3.8 \times 10^6$ from result (b). Moreover, with a more precise simulation, the octagonal shape had a higher quality factor of $Q = 8.0 \times 10^6$.

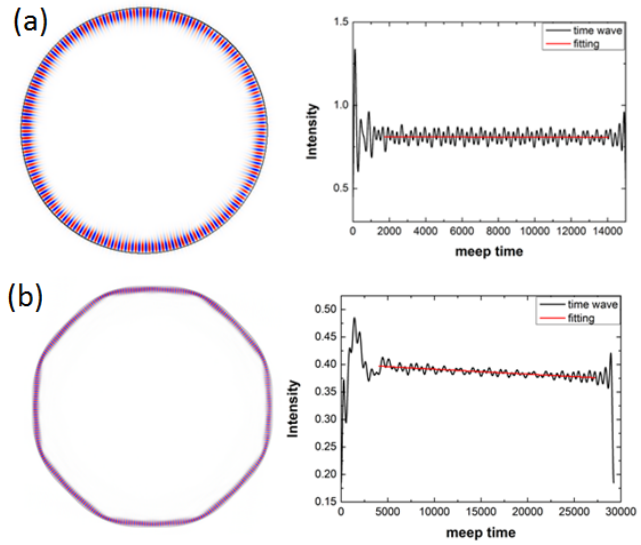

Fig. 6: Calculated H_z field profile of a circle (a) and an octagonal toroidal microcavity (b) by 2D-FDTD (left). Temporal decayed waveforms are shown on the right panels.

An octagonal shape has a smaller quality factor than a circular one, but the resonance profile is characteristic. As shown in Fig. 7, the evanescent field densities of a side part and a corner part are different. The silica toroid microcavity couples to a tapered fiber via the evanescent field, so the coupling rate depends on the strength of the evanescent field. Hence, an octagonal cavity may have degrees of freedom by selecting the contact location between the cavity and the tapered fiber.

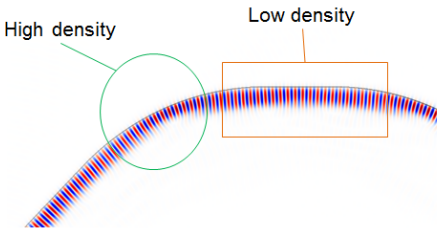

Fig. 7: The contrast of the degree of light leaking at a corner and a side of the octagonal cavity.

3.2 Coupled case

Next, I simulated about coupled cases. I assumed 1-μm tapered fibers as wave guides. In an octagonal shape, we employed two different contact points, a side and a corner. The results are shown in Fig. 8. The coupling coefficient was calculated by using coupled mode theory (CMT) [8].

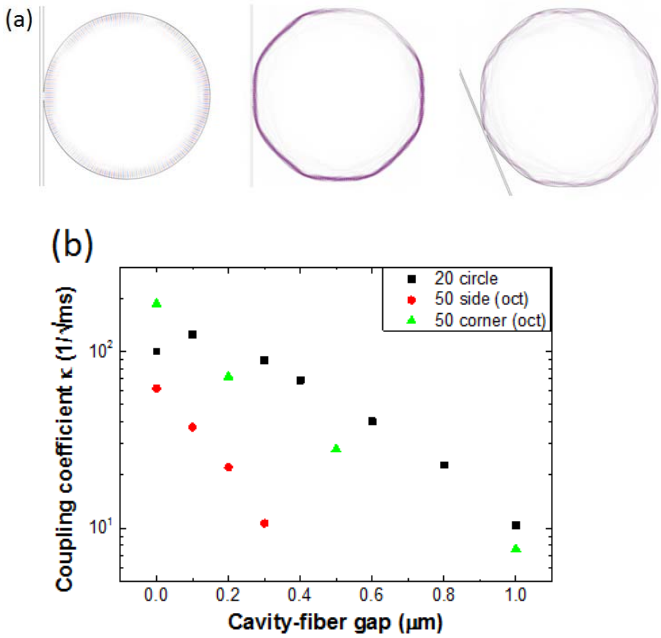

Fig. 8: (a) H_z field profile of a circle / an octagonal toroidal microcavity with tapered fiber. (b) Coupling coefficient vs. gap (square : r = 20 circlular, circle: r = 50, d = 10 octagonal side, triangle: r = 50, d = 10 octagonal corner).

These results indicate that we can change the coupling coefficient by changing the shape of a silica toroid microcavity. With an octagonal shape, we can obtain positive or negative coupling when we bring a tapered fiber in contact with the corner or side of a cavity, respectively. Therefore, we showed that a polygonal silica toroid has degrees of freedom as regards coupling with an evanescent coupler.

References

[1] A. M. Armani, R. P. Kulkarni, S. E. Fraser, R. C. Flagan and K. J. Vahala, Science **317,** 783 (2007).
[2] P. Del'Haye, A. Schliesser, O. Arcizet, T. Wilken, R. Holzwarth and T. J. Kippenberg, Nature **450,** 1214 (2007).
[3] W. Yoshiki, in *Annual report on Tanabe Lab* (2011).
[4] F. Xia, L. Sekaric, M. O'Boyle and Y. Vlasov, Appl. Phys. Lett. **89,** 041122 (2006).
[5] D.K. Armani, T. J. Kippenberg, S. M. Spillane and K. J. Vahala, Nature **42,** 925 (2003).
[6] C. Li and A. W. Poon, Opt. Lett. **30,** 546 (2005).
[7] C. Li, L. Zhou, S. Zheng and A. W. Poon, IEEE J. Quant. Elec. **12,** 1438 (2006).
[8] C. Manolatou, M. J. Khan, S. Fan, P. R. Villeneuve and H. A. Haus, IEEE J. Quantum Elec. **35,** 1322 (1999).

Construction of a microcavity measurement system and demonstration of an optical measurement

Yohei Ogawa (B4) and Hiroshi Kudo (B4)

A microcavity must be managed with fine control and observed with a camera if we are to measure its optical characteristics. We have designed and constructed a system for measuring microcavities.

Keywords：Optical measurement, Optical tapered fiber, Fine control

1. Optical characteristics of microcavity

An optical microcavity is an element that can trap light inside it. Its efficiency is expressed by a quality (Q) factor. To measure the Q factor, we must couple evanescent light into the microcavity. It is important that the distance between the microcavity and the optical waveguide is finely controlled. In this paper, we describe our construction of a fine control system for efficiently coupling light into a microcavity and our research on the optical measurement of microcavities.

2. Fine control system design

The measurement system we designed is shown in Fig. 1. The sample stage is automated for x- and y-axis with a precision of 10 nm. The tapered fiber stage is automated for the z-axis also with a precision of 10 nm. When we move the tapered fiber close to the microcavity, we need to observe the procedure from two directions. Moreover, since the input light wavelength is $\lambda = 1550$ nm we require an infrared (IR) camera. For these reasons, we observe upwards with an IR camera and from cross direction with a CCD camera to be close to both the tapered fiber and the microcavity.

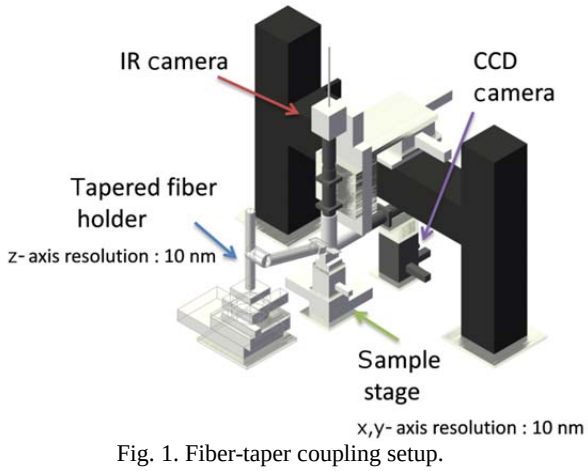

Fig. 1. Fiber-taper coupling setup.

3. Construction of the measurement setup

The measurement setup we constructed is shown in Fig. 2. We improved the system from section 2. First, we placed the system on a vibration removal board, which eliminated vibrations of over 0.5 Hz. Second, to exclude wind-induced vibration, we housed the system in an acryl box. Third, we rotated the tapered fiber stage 90 degrees from Fig. 1 to avoid the tapered fiber to interfere with the camera cylinder.

Fig. 2. Photograph of fiber-taper coupling setup.

4. Fixing optical tapered fiber

We need a fixing jig if we are to use optical tapered fiber in this centering system. We studied the two fixing methods shown in Fig. 3, namely straight fixing (Fig. 3(a)) and curved fixing (Fig. 3(b)).

The advantage of straight fixing is that it is easy to employ and the jig is easy to handle. However, we have to devise a method for measuring microcavities because a straight tapered fiber will introduce light into plural microcavities. There is other disadvantage that the straight fixing jig is larger than the curved one. This prevents it from being used in confined space of the centering system.

On the other hand, the advantage of curved fixing is that the curved tapered fiber can approach at a point. With this method, the transmitted light is localized outside the curved fiber. This enables us to measure microcavities with weak light. However, this fixing method is difficult to set up stably and is affected by vibration.

We tried using both fixing method and then selected

straight fixing jig and tried designing microcavities on a chip.

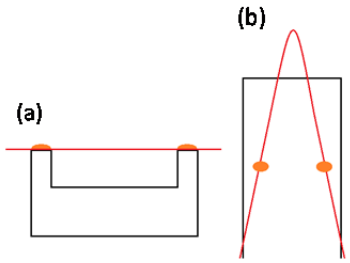

Fig. 3. Fixing fiber to jig. (a) Straight method. (b) Curve method.

5. Measurement of microcavity

We measured the optical characteristics of the microcavity with the system described in section 3. The microsphere cavity that we measured was made by heating a cut section of fiber using CO_2 laser, as shown in Fig. 4. The fiber diameter was about 300 μm. When we measured this microcavity, we obtained the transmission spectrum as shown in Fig. 4, whose Q factor is $Q = 5 \times 10^5$. This result means that we can measure $Q < 10^5$ with this centering system. Currently we are improving the wavelength accuracy and trying to enable a measurement of $Q = 10^8$, that is required for a silica toroid microcavity measurement.

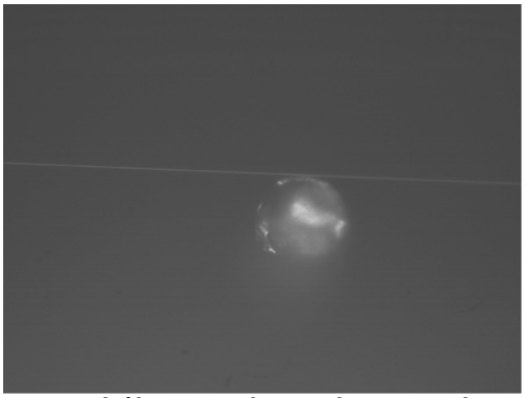

Fig. 4. Tapered fiber is touching with a microsphere. Fiber diameter is about 2 μm; microsphere diameter is about 300 μm.

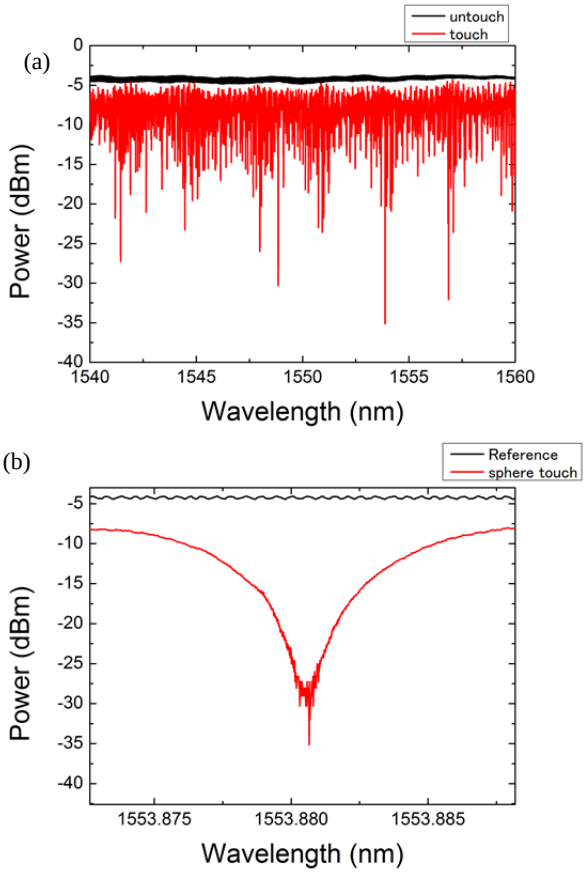

Fig. 5. (a) Transmission of tapered fiber touching microsphere. (b) Zoomed dip at $\lambda = 1553.881$ nm. Loaded Q-factor is $Q = 5 \times 10^5$.

6. Conclusion

In this paper, we designed and constructed a tapered fiber alignment system and we successfully measured $Q = 10^5$ from a $d = 300$ μm microsphere. We will improve this measurement system with the aim of using it to measure $Q = 10^8$ for application to silica toroid microcavities.

7. Reference

[1] S.M. Spillane, T. J. Kippenberg, O. J. Painter and K. J. Vahala, *Phys. Rev. Lett.* **91**, 043902 (2003)

Fabrication of whispering gallery mode resonator by laser heated pedestal growth method

Hiroshi Kudo (B4)　Yohei Ogawa (B4)

We attempted to fabricate whispering gallery mode resonators made of sapphire using the laser heated pedestal growth (LHPG) method. As a result, we successfully fabricated a resonator with a Q of 350. Also, we found that the resonator's shape is controlled by controlling the velocity ratio and also by controlling the laser output.

Key words: Crystal growth, whispering gallery mode, laser heated pedestal growth

1. Abstract

The laser heated pedestal growth (LHPG) method is a technique that employs the Czochralski (CZ) method, which was developed for manufacturing fiber lasers [1]. In our fabrication process, we melt the feed rod with a CO_2 laser instead of the crucible of the CZ method. Here, we demonstrate that we can control the resonator shape by controlling the velocity ratio of the seed rod, feed rod and the feed rod diameter, as shown in Eq. (1) [2].

$$\frac{d_2}{d_1} = \frac{\sqrt{v_1}}{\sqrt{v_2}} = \sqrt{v_{\text{rate}}} \qquad (1)$$

d_1: Feed rod diameter
d_2: Seed rod diameter
v_1: Feed rod velocity
v_2: Seed rod velocity

By changing the ratio of v_1 and v_2 on the way, we can fabricate a bulge, which is used as a WGM microcavity.

2. Experimental procedure

Here, we describe four experimental methods, which we used for the following purposes.

1. Identification of CO_2 laser power and the velocity of each rod.
2. Shape change by τ when velocity ratio is 1:3.
3. Shape change by CO_2 laser power P.
4. Optical measurement.

1. Identification of crystal growth condition

(a) Place a feed rod in the concentrated zone of the CO_2 laser.
(b) Melt the tip of the feed rod with the CO_2 laser.
(c) Attach the feed rod and a seed rod.
(d) Pull both rods upward. Here, the feed velocity is 0.12 mm/min and the seed velocity is 0.72 mm/min.

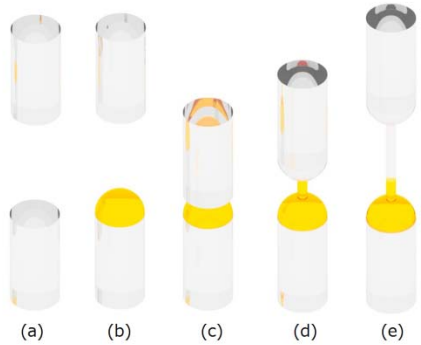

Fig. 1: Crystal fiber fabrication process with laser heated pedestal growth method.

2. Shape change by the duration τ when v_{rate} is 1:3. (v_{rate} :1:6 →1:3.)

(a) The same as 1. (d).
(b) Decelerate the seed rod velocity at 0.36 mm/min for duration time τ.
(c) Stop the feed rod and then pull the seed rod at a velocity of 0.12 mm/min downward.

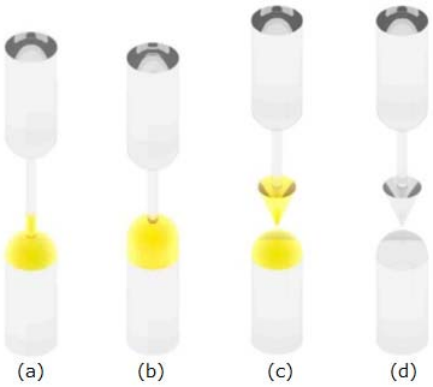

Fig. 2: Modified laser heated pedestal growth for whispering gallery mode cavity fabrication.

3. Shape change by changing CO_2 laser power P.

(a) The same as 1. (d).
(b) Decelerate the seed rod velocity at 0.24 mm/min for 100 sec.
(c) Stop both rods and increase the CO_2 laser power. Here, we use P as the CO_2 laser

power.

(d) With the feed rod stopped, then pull the seed rod at a velocity of 0.12 mm/min downward.

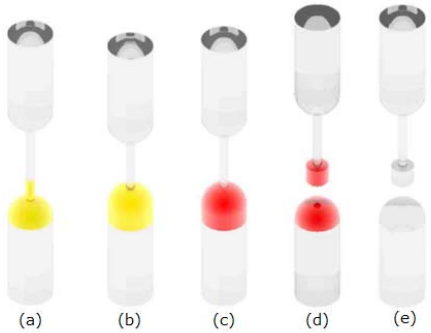

Fig. 3: Whispering gallery mode cavity fabrication process when laser power is changed during the process.

4. Optical measurement

As shown in Fig. 4, we performed an optical measurement of the fabricated microcavities.

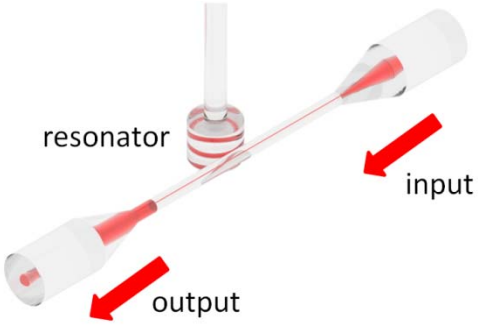

Fig. 4: Schematic illustration of tapered fiber optical measurement setup.

3. Experimental result

1. Identification of crystal growth condition

Theoretically the fabricated fiber diameter is 173μm from Eq. (1), because v_{rate} is 1:6, and the feed rod diameter is 425 μm. Here we evaluated the crystal growth condition in terms of the velocity of both rods and CO_2 laser power. Furthermore, the crystal growth condition can be divided into the following five stages.

Very good : Appropriate crystal growth continues for some minutes, and the two rods adhere for 5 minutes.

Good : Appropriate crystal growth continues for some minutes, but the two rods separate within 5 minutes.

Average : Appropriate crystal growth is impossible. The grown crystal becomes gradually thinner and the two rods separate.

Poor : A crack appears in the grown crystal, but crystal growth is possible.

Very poor : Crystal growth is impossible.

From the result, we determined that better crystal growth can occur at the dotted line in Fig. 5. Therefore, we fabricated the microcavities in the range indicated by the green arrow.

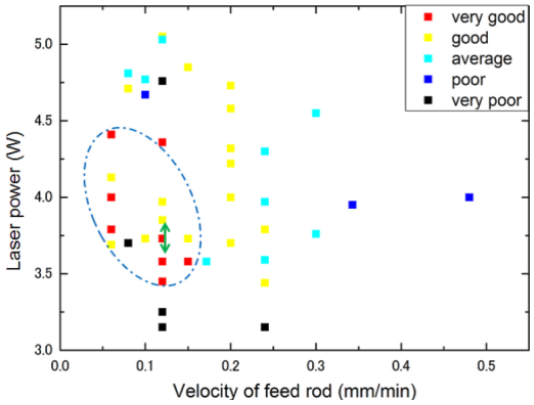

Fig. 5: Crystal growth conditions at different rod speeds and powers.

2. Microcavity shape change with duration τ when v_{rate} is 1:3.

From experimental procedure 2, we found that the fabricated microcavities shape depends on τ as shown in Fig. 6. And, Fig. 7 indicates the aspect ratio, the length and the width of the each microcavity.

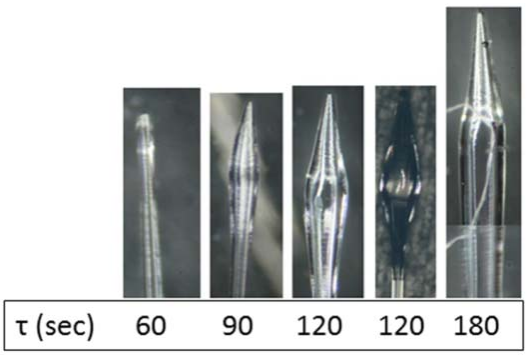

Fig. 6: Fabricated microcavities with different τ's.

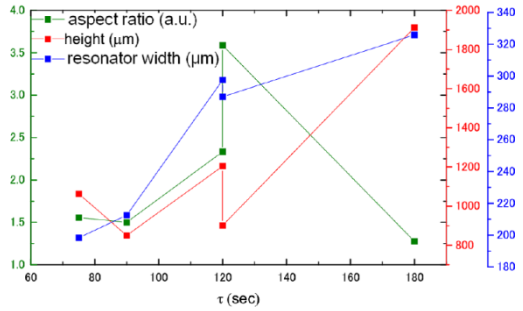

Fig. 7: The aspect ratio, the length and the width of the fabricated microcavities with different τ's.

3. Microcavity shape dependence on CO_2 laser power.

From experimental procedure 3, we found that the fabricated microcavities shape depends on P as shown in Fig. 8. And, Fig. 9 indicates the aspect ratio, length and width of the fabricated microcavities.

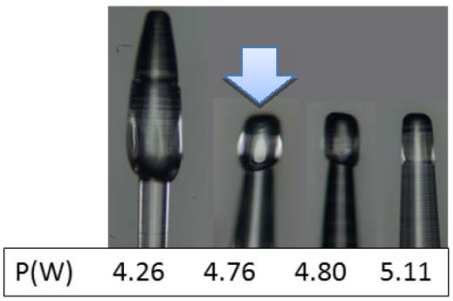

Fig. 8: Fabricated microcavities with different Ps.

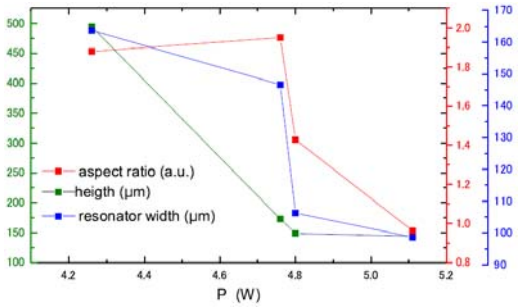

Fig. 9: Aspect ratio, length and width of fabricated microcavities at different P values.

4. Optical measurement

When we performed an optical measurement on the fabricated microcavities (indicated by arrow in Fig. 8), we obtained the result shown in Fig. 10, which gave a Q of 350.

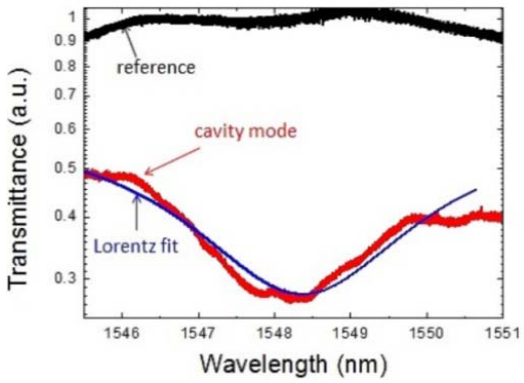

Fig. 10: Transmittance spectrum measured with tapered fiber setup.

4. Discussion and summary

From the above results, we consider the aspect ratio of the fabricated microcavities to be the best whenτ is equal to 120 sec. Also, although we could reduce the volume of the fabricated microcavities by enhancing the CO_2 laser power, the aspect ratio also became lower. This result shows that the volume and the aspect ratio are in a trade-off relationship in this method. Finally, we performed an optical measurement of the fabricated microcavities, and found that a Q of 350. From the above, we confirmed the usefulness of this microcavity fabrication technique using crystal growth. As future work, we aim to improve the measurement system, make the cavity shape more symmetrical, and reduce the microcavity volume.

References

[1] A. Yokoo, S. Tomaru, I. Yokohama, H. Itoh, T. Kaino, "A new growth method for long rod like organic nonlinear optical crystals with phase-matched direction," J. Cryst. Growth **156,** 279 (1995).

[2] M. M. Fejer, J. L. Nightingale, G. A. Magal, and R. L. Byer, "Laser-heated miniature pedestal growth apparatus," Rev. Sci. Instrum. **55**, 11 (1984).

Statistical data

Publications

(April 2011 – March 2012)

Journal Papers:

[1] A. Yokoo, T. Tanabe, E. Kuramochi, and M. Notomi,"Ultrahigh-Q nanocavities written with a nanoprobe," Nano Lett. Vol. 11, No. 9, pp. 3634-3642 (2011).

[2] M. Notomi, A. Shinya, K. Nozaki, T. Tanabe, S. Matsuo, E. Kuramochi, T. Sato, H. Taniyama and H. Sumikura, "Low power nanophotonic devices based on photonic crystals towards dense photonic network on chip," IET Circuits, Devices & Systems, Vol. 5, No. 2, pp. 84-93 (2011).

International Conferences:

[1] K. Nozaki, T. Tanabe, A. Shinya, S. Matsuo, T. Sato, Y. Kawaguchi, H. Taniyama, and M. Notomi, "Photonic crystal nanocavities toward low-power on-chip nanophotonic devices," IQEC/CLEO Pacific Rim, 4630-IT-5, Sydney, August (2011).

Awards:

20. April, 2011 Takasumi Tanabe

The Commendation for Science and Technology by the Minister of Education, Culture, Sports, Science and Technology (The Young Scientists' Prize)

18. Jun, 2011 Takasumi Tanabe

Ando Incentive Prize for the Study of Electronics

Theses

Bachelor theses

Yohei Ogawa, “Optical measurement of an optical microcavity using a tapered optical fiber”

Takumi Kato, “Study on the fabrication of polygonal silica toroid microcavities”

Hiroshi Kudo, “Study on the fabrication of a whispering-gallery mode cavity using laser heated pedestal growth”

Wataru Yoshiki, “Study on a bistable memory using the optical Kerr effect in a silica toroid microcavity”

Keio University Special Grant-in-Aid for Innovative Collaborative Research

Development of noble photonic technologies by exploring extended nano-space processing

A new project “Development of noble photonic technology by exploring extended nano-space processing” has started as a mini-COE type research funding. By using microcavity as a core technology, we try to use *extended nano-space* with close collaboration between photonics, precise machining, and biology.

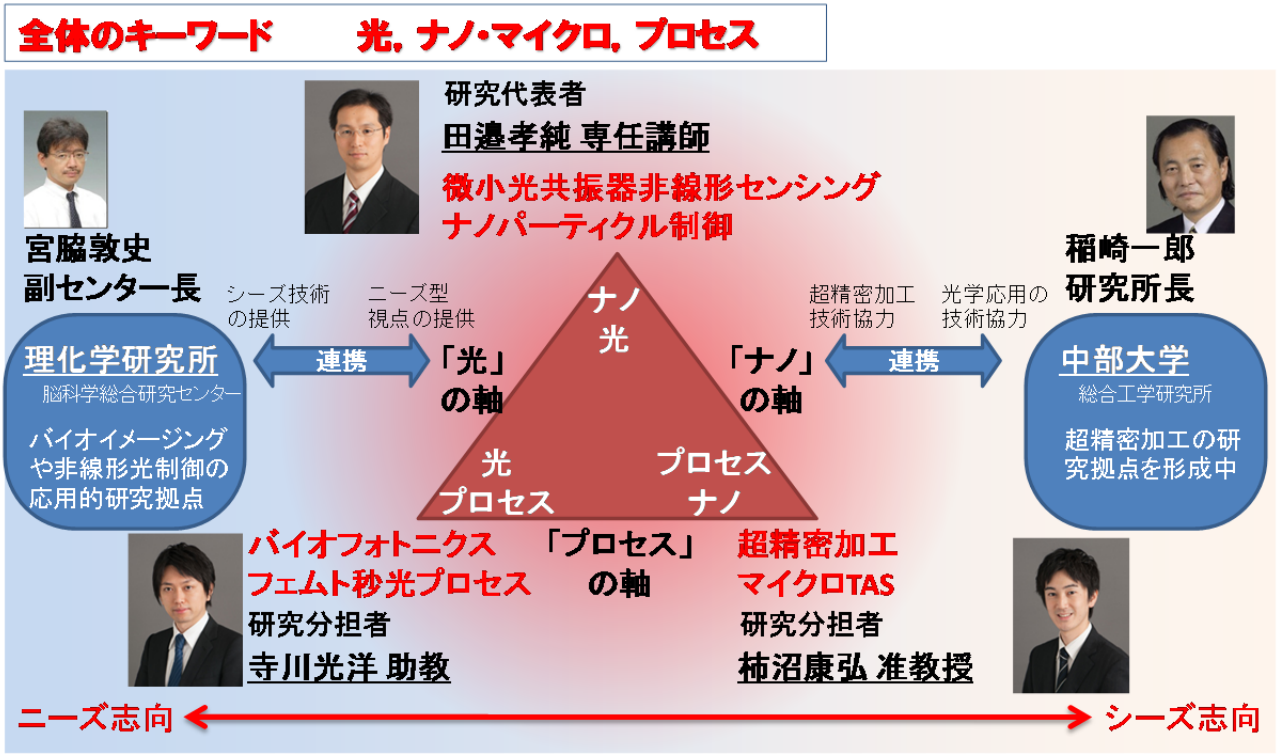

Activity reporting 2011:

27. July (Wed.)	Kick-off meeting of the research project
	Sharing the goal of the project
	Research meeting with three groups in Keio University
30. Nov. (Wed.)	Research interchange between 3 groups in Keio University (Lab tours)
27. March (Wed.)	A meeting to report results of year 2011

A gathering for young photonic researchers in Keio University

We held a gathering for young researchers in Keio University who works in the field of optics and photonics. Participants are faculties and students from 6 laboratories; Prof. Yoshihiro Taguchi's Lab. (System design), Prof. Junko Ishii-Hayase's Lab. (Applied physics), Naoki Yamamoto's Lab. (Applied physics), Prof. Shinichi Watanabe's Lab. (Physics), Prof. Mitsuhiro Terakawa's Lab. (EEE), and Prof. Takasumi Tanabe's Lab. (EEE).

Report:

Date: 16. September (Friday) 15:30-
Place: Discussion room 7 (14-217), poster took place in Forum Space in 7'floor
Title: A gathering for young photonic researches in Keio University

15:30 Preface (Tanabe)
15:35 Introduction of Yamamoto group (Quantum optics)
15:50 Introduction of Watanabe group (Optical physics / Terahertz physics)
16:05 Introduction of Hayase group (Quantum optics)
16:20 Break (10 min.)
16:30 Introduction of Tanabe group (Electro-optics)
16:45 Introduction of Taguchi group (Optical MEMS)
17:00 Introduction of Terakawa group (Bio-photonics)
17:15 Introduction of students and short presentations (1 min. x 19)
17:45 Break & Move room
17:50 - 18:50 Poster presentation by students @ Forum Space in 7'th floor